Temporal Scaling of Streamflow Elasticity to Precipitation: A Global Analysis

AGU ADVANCING EARTH AND SPACE SCIENCE

Water Resources Research

RESEARCH ARTICLE
10.1029/2021WR030601

Temporal Scaling of Streamflow Elasticity to Precipitation: A Global Analysis

Yongqiang Zhang[1], Alberto Viglione[2], and Günter Blöschl[3]

[1]Key Laboratory of Water Cycle and Related Land Surface Processes, Institute of Geographic Sciences and Natural Resources Research, Chinese Academy of Sciences, Beijing, China, [2]Department of Environment, Land and Infrastructure Engineering, Politecnico di Torino, Torino, Italy, [3]Institute of Hydraulic and Water Resources Engineering, Technische Universität Wien, Vienna, Austria

Abstract Streamflow elasticity to precipitation, defined as the percent change of streamflow resulting from a 1% change in precipitation, is sometimes used as an alternative to rainfall-runoff models in climate impact analyses. Elasticity is usually estimated from long streamflow and precipitation series aggregated at annual time steps while the climate impact analyses are usually geared toward changes at decadal scales. The purpose of this paper is therefore to understand how the elasticity depends on the aggregation time scale and the process controls of such a dependence. We analyze streamflow records of 7,053 catchments around the world over the period 1950–2016, and select 5,327 with reliable elasticity estimates for aggregation time ranging from 13 to 60 months. We find a significant scaling of streamflow elasticity to precipitation with aggregation time in 66% of the catchments which is much larger than expected by chance. Positive scaling occurs much more frequently than negative scaling. More arid/less rainy catchments, less forested catchments and catchments with a large base flow contribution to streamflow are more frequently characterized by a positive scaling. A random forest classification model identifies aridity index, latitude, mean annual precipitation, the potential evapotranspiration seasonality, the base flow index and the precipitation seasonality as relevant explanatory variables of the scaling. We interpret the sign of the scaling by non-linear runoff generation in arid regions, by the effect of climate modes and snow processes, and by the regulation capacity of vegetation to transpire more water if the past years were wet. It is suggested to use decadal elasticities instead of annual elasticities in climate impact analyses in order to account for their scaling behavior.

Key Points:

- Streamflow elasticity to precipitation depends significantly on aggregation time in 66% out of the 5,327 global catchments
- Catchments that are arid or little forested, or possess gentle catchment slope tend to exhibit positive scaling
- Decadal streamflow elasticity to precipitation should be used instead of annual elasticities in climate impact analyses

Correspondence to:
Y. Zhang,
zhangyq@igsnrr.ac.cn

Citation:
Zhang, Y., Viglione, A., & Blöschl, G. (2022). Temporal scaling of streamflow elasticity to precipitation: A global analysis. *Water Resources Research*, *58*, e2021WR030601. https://doi.org/10.1029/2021WR030601

Received 10 JUN 2021
Accepted 14 JAN 2022

Author Contributions:
Conceptualization: Yongqiang Zhang, Alberto Viglione, Günter Blöschl
Formal analysis: Yongqiang Zhang
Investigation: Yongqiang Zhang
Methodology: Yongqiang Zhang, Alberto Viglione, Günter Blöschl
Writing – original draft: Yongqiang Zhang, Alberto Viglione, Günter Blöschl
Writing – review & editing: Yongqiang Zhang, Alberto Viglione, Günter Blöschl

1. Introduction

Climate change is expected to modify streamflow through changes in the precipitation regime and evaporation (IPCC, 2013). These impacts are usually assessed on the basis of a modeling cascade consisting of global climate models, regional climate models, and rainfall-runoff models (Teutschbein & Seibert, 2010). The latter are subject to considerable uncertainty, in particular for representing changing conditions, due to two main reasons. First, when using empirical rainfall-runoff models, model parameters are not directly measurable because of the underlying spatial variability that is not commensurate with current field measurement methods (Peters-Lidard et al., 2017). Second, catchments tend to co-evolve with climate in a coupled system thus resulting in an aggregate behavior that differs from that at the local scale or laboratory scale (Blöschl et al., 2013). Because of these uncertainties, alternative, data-based approaches have been developed to quantify future changes of streamflow in response to changes in the climate regime. One such approach is the concept of elasticity, that is,, a measure of a variable's sensitivity to a change in one or more other variables (Liu et al., 2017; Nemec & Schaake, 1982). One of the possible definitions of streamflow elasticity is the percent change of streamflow resulting from a 1% change in precipitation or other climate variables. Since this definition is straightforward, it is widely used for climate change and water resource management studies (Bao et al., 2012; Huang et al., 2016; Liang et al., 2015; Lv et al., 2018; NĚMec & Schaake, 1982).

The elasticity is a lumped representation of the hydrological effects of a multitude of processes affecting the response of streamflow to variations in climate variables. One would therefore expect it to depend on both climate variables and catchment attributes. Specifically, for the case of streamflow elasticity to precipitation, numerous studies have indeed identified these controls in various setting. Sankarasubramanian et al. (2001), for example, estimated streamflow elasticity to precipitation for the United States and found it to generally range from 1.0 to 2.5. They found the highest elasticities in the arid and semi-arid regions of the Midwest and Southwest while

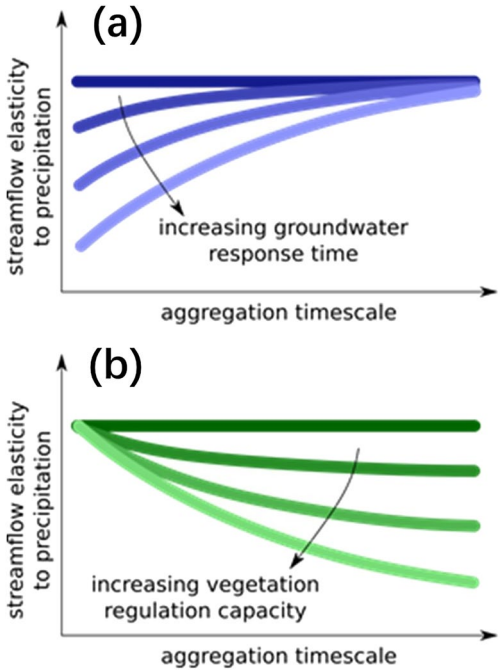

Figure 1. Schematic representation of how streamflow elasticity to precipitation may depend on the aggregation timescale. The two panels show hypothetical dependences of elasticity to the groundwater response time (Figure 1a) in a catchment where the contribution of groundwater to streamflow is significant, and of vegetation regulation capacity (Figure 1b) in a catchment where vegetation metabolism is significant.

catchments with generally high moisture showed rather low elasticities as did catchments where snow processes played a role. Chiew (2006) and Chiew et al. (2006) found streamflow elasticity to precipitation in Australia to be closely related to the runoff coefficient (ratio of average annual streamflow and precipitation). For example, typical elasticities were around 1.5 and 5.0 in catchments with runoff coefficients of 0.6 and 0.01, respectively. He interpreted the higher sensitivity of streamflow to precipitation in catchments with low runoff coefficients by the non-linearity in the precipitation runoff process, as the same absolute change in streamflow for a given absolute change in rainfall would be reflected as a higher elasticity in catchments with a low runoff coefficient. The elasticity - runoff coefficient relationship also translated in correlations of elasticity with precipitation and aridity. On the other hand, weaker (and also negative) correlations were found with percentage of woody vegetation in the catchment and the soil plant water holding capacity. These relationships were confirmed in a similar global study (Chiew, 2006) that identified the highest elasticities in Southeast Australia and South and West Africa, and the lowest elasticities in southwestern South America and in middle and high latitudes in the Northern Hemisphere for similar process reasons.

Elasticities can be either estimated on the basis of rainfall-runoff models of various complexity or by parametric or non-parametric estimators directly from the streamflow and precipitation data (Andreassian et al., 2016; Liu et al., 2017). The various methods have their relative strengths and weaknesses, mainly related to the model assumptions and the various levels of robustness. Irrespective of the specific estimation method, the elasticity is almost always estimated from streamflow and climate data at the annual time scale, and the year-to-year variability of these data is interpreted as being representative of the catchment response to climate variability Sankarasubramanian et al., (2001). If the elasticity so estimated is applied to assess potential climate change response at the decadal scale there is an implicit assumption that the elasticity does not depend on the time scale, that is, streamflow response to annual climate fluctuations is identical to streamflow response to, say, decadal climate fluctuations. Annual streamflow elasticity has been used to quantify the impacts of climate on streamflow for several decades (G. Y. Zhou et al., 2015; Milly et al., 2005; Sankarasubramanian et al., 2001; Ukkola et al., 2016; Zheng et al., 2009). The elasticity, however, may in fact depend on the time scale. For example, an anomalously wet annual period may transform in a larger or smaller streamflow increase than an anomalously wet decade. In a changing climate where variables change dynamically at various time scales, it may therefore be more relevant to consider elasticity conditional on the time scale of interest.

The elasticity is controlled by different hydrological processes at different temporal scales. At monthly or seasonal scale, portions of the precipitation during precipitation events are stored in the pores and fractures of the subsurface media as groundwater storage, which gradually contributes baseflow to the total streamflow. Groundwater storage buffers streamflow response to high frequency climate variability, enhancing streamflow resilience to climate change (Andermann et al., 2012; Berghuijs et al., 2016; Condon & Maxwell, 2019; de Graaf et al., 2019; Maxwell & Condon, 2016; Scanlon et al., 2005, 2018). At annual to multiannual scales, precipitation is widely considered the dominant factor because of its large contribution to streamflow (Fu et al., 2007; Sankarasubramanian et al., 2001; Zheng et al., 2009) but there are a number of possible reasons to expect that the elasticity can be time scale dependent even when considering annual, multiannual and decadal scales: for example, groundwater contribution, snowmelt, vegetation metabolism and climate oscillation. Where groundwater contributes significantly to streamflow, one may expect the sensitivity of streamflow to precipitation is higher at timescales commensurate with the groundwater response time (Figure 1a). In high latitudes or high altitudes, streamflow is largely influenced by snowmelt, which tends to change oppositely to precipitation under climate variability since higher precipitations tend to be associated with lower temperature and thus less snow melt (Z. Li et al., 2020) thus resulting into low or even negative elasticities at timescales commensurate with climatic fluctuations. Vegetation metabolism can potentially contribute to temporal scaling of the elasticity since vegetation tend to transpire more

water if the past seasons (or years) are wet and vice versa, showing annual to interannual regulation capacity (Bott et al., 2006). One would therefore expect that the sensitivity of streamflow to precipitation decreases at increasing timescales for which optimisation of transpiration occurs (with effects on the elasticity shown in Figure (b). Also, climate tends to oscillate, in a quasi-period way, at many different time scales. This includes the El Niño Southern Oscillation (ENSO) phenomenon fluctuating at the scale of two to 7 years (Timmermann et al., 2018), the North Atlantic Oscillation (NAO; Folland et al., 2009; Hofstatter & Bloschl, 2019) and the Pacific Decadal Oscillation (PDO; S. J. Li et al., 2020) that fluctuate at a decadal scale and affect Europe and North America. How the above-mentioned forcing variables may affect the scaling of streamflow elasticity to precipitation with aggregation time will depend on how catchments respond to such forcings.

Indeed, also streamflow has been found to oscillate at many different time scales, although the seasonal (within year) streamflow variability often is much more pronounced than other time scales. Because of this, streamflow usually exhibits a multiscale, fractal characteristic (Markonis et al., 2018). This behavior may be partly inherited from the multiscale climate and another part may be due to the catchment processes. For example, Szolgayova et al. (2014) and Markonis et al. (2018) found catchment area and aridity to explain well the Hurst coefficient, which is an index representing the power law dependence of the streamflow variability with time scale. This explanatory power was interpreted as the effect of catchment storage, in particular in the groundwater and in lakes on the memory of streamflow which may be more pronounced for larger catchments, where the subsurface contribution to streamflow is usually larger than in small catchments.

This time scale dependence of hydrological response can be clearly seen in the propagation of droughts in the hydrological cycle (Apurv et al., 2017; Tallaksen et al., 2009; Van Loon & Laaha, 2015). The main mechanisms tend to be the storage of water in the subsurface as well as travel times of water from the land surface to the subsurface, both mechanisms delaying the climate time scales and thus introducing longer time scales into hydrological response. On the other hand, there may also be non-linear interactions within catchments that introduce time scales that are not present in the climate signal through processes of co-evolution (Sivapalan & Bloschl, 2015). These interactions may occur at the scale of events where event-scale rainfall and seasonal soil moisture are coupled and longer scales of soil and vegetation evolution over decades, as well as groundwater flow interacting with climate controls (Troch et al., 2015). The non-linearity can be due to the coupling of linear or non-linear processes or threshold processes that may result in bistable system states, where the state (e.g., wet or dry) can switch from one state to another, leading to an abrupt change in the regime (Scheffer et al., 2009). An example of a bistable system is the interaction between transpiration and saline groundwater, as proposed by (Peterson et al., 2009). Vegetation can play a key role in both adapting to and modulating the soil moisture regime (Asbjornsen et al., 2011; D'Odorico et al., 2007) resulting in complex interactions and feedbacks between vegetation and hydrologic flows at multiple scales. These interactions include the ability of plants, at least in some instances, to engineer their soil characteristics and to learn from the past climate in order to maximize biomass growth and survival chances (Gao et al., 2014).

All of these potential processes may interact and their relative importance may depend on the particular climate, vegetation, soil, landform and geological conditions. At this stage it is not clear how exactly the elasticity depends on time scale and what the processes controls of such a dependence are. This study mainly focuses on annual to multiannual (five years) scale. The aim of this paper is therefore (a) to identify the dependence of elasticity on timescale based on a global streamflow data set, and (b) to attribute this dependence to any process causes.

2. Data and Methods

2.1. Data

Streamflow and precipitation data used in this study were obtained from the following sources. We used monthly streamflow data from seven sources, including the Global Runoff Data Centre (GRDC, located in Germany, http://www.bafg.de/GRDC/EN/Home/homepage_node.html), (b) the U.S. Geological Survey (USGS) National Water Information System and Geospatial Attributes of Gages for Evaluating Streamflow (GAGES)-II database, (c) the Australian Bureau of Meteorology (http://www.bom.gov.au/water/hrs/), (d) the HidroWeb portal of the Brazilian Agência Nacional de Águas (http://www.snirh.gov.br/hidroweb), (e) the European Water Archive of the European Flow Regimes from International Experimental and Network Data (EURO-FRIEND-Water; http://ne-friend.bafg.de) and the Catchment Characterization and Modeling–Joint Research Centre database, (f) the Water

Table 1
Percentiles of the 17 Catchment Attributes of the 7,053 Gauged Catchments Used in This Study

Attribute	Unit	Min	2.5th	25th	Median	75th	97.5th	Max
Latitude	Degree	−45.6	−36.7	35.2	40.9	47.0	59.7	72.2
Catchment size	km^2	1.9	22.1	179.7	547.0	1,660.0	7,535.7	9,981.2
Mean elevation	m a.s.l	11.3	39.1	251.8	468.4	1,019.1	2,935.0	4,285.9
Mean slope	Degree	0.03	0.23	0.48	1.16	2.41	5.19	9.08
Permeability	log*k* (m^2)	4.80	4.95	4.95	5.95	7.22	8.21	8.44
Runoff coefficient	Unitless	0.00	0.01	0.25	0.38	0.53	1.05	1.25
Mean annual precipitation	mm/year	40	273	561	904	1,165	1,886	3,231
Ratio of summer precipitation to winter precipitation	Unitless	0.00	0.04	0.86	1.41	2.39	17.87	2,002.30
Ratio of summer potential evaporation to winter potential evaporation	Unitless	0.72	1.27	3.02	5.16	9.05	34.34	132.71
Aridity index	Unitless	0.1	0.4	1.0	1.2	1.9	5.3	79.7
Mean annual air temperature	℃	−13.15	−0.85	5.69	9.07	13.35	21.92	27.26
Snow fraction	Unitless	0.00	0.00	0.01	0.11	0.28	0.58	0.97
Permafrost fraction	Unitless	0.00	0.00	0.00	0.00	0.00	0.15	0.95
Forest fraction	Unitless	0.00	0.00	0.01	0.14	0.53	0.98	1.00
Shrubland fraction	Unitless	0.00	0.00	0.00	0.00	0.00	0.22	1.00
Savannas fraction	Unitless	0.00	0.00	0.07	0.25	0.50	0.86	0.99
Grassland fraction	Unitless	0.00	0.00	0.01	0.04	0.24	0.93	1.00
Leaf area index	Unitless	0.00	0.12	0.80	1.31	1.90	3.50	5.23

Survey of Canada Hydrometric Data (HYDAT; https://www.canada.ca/en/environment-climate-change), and (g) the Chilean Center for Climate and Resilience Research (CR2; http://www.cr2.cl/datos-de-caudales/) and Catchment Attributes and Meteorology for Large-Sample Studies (CAMELS-CL). To have high quality streamflow data set, we setup the following selection criteria, including (a) largely unregulated (reservoir capacity less than 10% of total annual streamflow, according to Zhou et al. (2021)), (b) largely un-irrigated (irrigation area is less than 10% of total catchment area), (c) with small or negligible water body (less than 10% of catchment area), (d) small to median size (less than 10,000 km^2), and (e) having more than 30 years of streamflow observations for the period from 1950 to 2016. Based on the above-mentioned criteria, we selected 7,053 out of 21,953 catchments. The original streamflow data is with daily resolution. We used daily streamflow to convert to monthly values by arithmetical average, and a maximum of two missing days was allowed. As a result, 50% of the 7,053 catchments have 48–67 years of streamflow observations, 25% of the catchments have 37–48 years of observations, and 25% of the catchments have 30–37 years of observations in 1950–2016. Daily precipitation data from 1948 to 2016 were obtained from the 0.25° resolution Princeton Global Forcing (PGF) data (Sheffield et al., 2006, 2012). The gridded precipitation data were aggregated to each catchment using area weighting average, based on grid cells and their area percentage within the target catchment.

Additionally, to estimate/predict the elasticity, the scaling magnitude and scaling signs, we used 17 catchment attribute data for the 7,053 gauged catchments from the following sources: (a) the ALOS World 3D DSM data set with 30m resolution was used for calculating catchment size, elevation and slope (Takaku et al., 2014), (b) soil permeability (the ease of fluid flow through soil porous media) was obtained from Global Hydrogeology Maps (Gleeson et al., 2014), (c) climatological data such as mean annual precipitation, precipitation seasonality and potential evaporation seasonality, and aridity index were calculated from PGF data set (Sheffield et al., 2006, 2012), (d) land cover type data were obtained from 2001 MODIS yearly land cover type (https://doi.org/10.5067/MODIS/MCD12Q1.006), and (e) leaf area index data were derived from the Advanced Very High Resolution Radiometer (AVHRR) Global Inventory Modeling and Mapping Studies (GIMMS) LAI3g version 2 (https://daac.ornl.gov/VEGETATION/guides/Mean_Seasonal_LAI.html). Table 1 summarizes statistical details of each catchment attribute from the 7,053 selected gauged catchments. Note that precipitation information is used for calculating the elasticity and predicting the scaling of elasticity. The elasticities are calculated using the

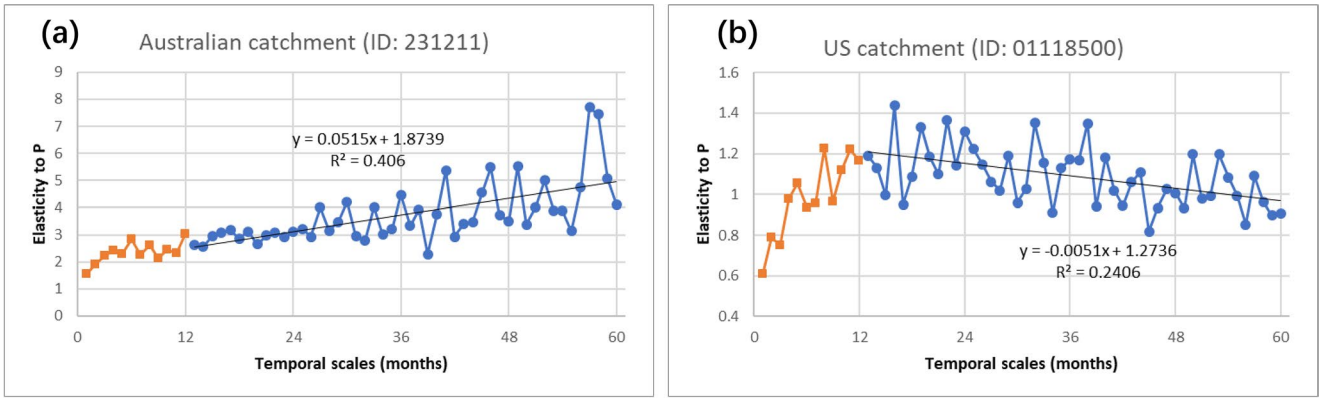

Figure 2. Elasticities of two example catchments for different aggregation times (from 1 month to 60 months). All the elasticities shown in the examples pass the F test ($p < 0.1$). Regression line indicates the scaling for aggregations from 13 to 60 months (a) Is the Lerderderg river catchment at Goodman creek (235 km^2) in Victoria, Australia which has a positive scaling, (b) is the Pawcatuck river catchment at Westerly (766 km^2) in Connecticut, US which has a negative scaling.

fluctuations or deviations from precipitation averages, while the prediction of the scaling of elasticity is done using long term precipitation attributes, such as mean annual precipitation and ratio of summer precipitation to winter precipitation.

2.2. Methods

We assume that variability of streamflow at a temporal aggregation interval i (e.g., annual) is mainly influenced by the variability in precipitation at that aggregation interval. Therefore, we can estimate streamflow variability at aggregation interval i (dQ_i, streamflow anomaly defined as $Q_i - Q$) using the following equation:

$$dQ_i = \frac{\partial Q}{\partial P} dP_i \tag{1}$$

which can be rewritten as

$$\frac{dQ_i}{Q} = \frac{\partial Q}{\partial P}\frac{P}{Q}\frac{dP_i}{P} = \frac{\partial Q/Q}{\partial P/P}\frac{dP_i}{P} = \varepsilon_{P_i}\frac{dP_i}{P} \tag{2}$$

where Q is the mean streamflow at aggregation interval i, P is the mean precipitation at aggregation interval i, and ε_{P_i} is the streamflow elasticity to precipitation. Therefore, ε_{P_i} is calculated as the slope of a linear regression line fitted to monthly data (and aggregations of them) of deviations of precipitation from the mean (dP_i) divided by mean precipitation (P) as independent variable and of deviations of streamflow from the mean (dQ_i) divided by mean streamflow (Q). It is noted this study used calendar year for the temporal aggregation. Since this is a global data analysis, we attempt to simplify our analysis using consistent time period. However, we acknowledge that using the hydrological year may be a better choice for a local analysis.

To avoid unreliable ε_{P_i} estimates, we use the F-test to test validity of the linear regression in Equation 2, only select the ε_{P_i} estimates with $p < 0.1$, and treat the rest as unvalidated and not used for calculating scaling. Since there are 48 aggregation intervals from 13 to 60 months for each catchment, and we only select the catchments with more than 36 validated ε_{P_i} estimates (i.e., more than 75% data) for calculating the scaling of ε_{P_i}. As a result, there are 5,327 catchments finally selected for the following analysis.

The scaling of ε_{P_i} is also estimated as a linear trend of ε_{P_i} as a function of the aggregation time intervals from 13 to 60 months. Even though the scaling of ε_{P_i} is not expected to be linear (see e.g., Figure 1), we use here a linear model to detect a tendency in a parsimonious way. The estimates of the scaling of ε_{P_i} are given by the slope of the regression line between elasticity and aggregation times equal or larger than one year (Figure 2), obtained using the ordinary least squares (OLS) method because of its simplicity. The OLS method returns almost identical results of the scaling, compared to a more complex method, such as the Mann-Kendall test with the Sen slope ($R^2 = 0.996$), demonstrating the robustness of the OLS method. Figure 2 illustrates the scaling of ε_{P_i} for two randomly selected catchments with positive and negative scaling. The example of Figure 2a is located in Victoria,

Australia, with 235 km^2 catchment area. In this catchment the elasticity increases with time scale, from 2.5 at one year to around 5 for five years, and the scaling value is 0.05 per year. On the other hand, a forest catchment (77.6% forest cover) in Connecticut, US, shows the opposite behavior (Figure 2b). While at a time scale of a year the elasticity is around 1.2, it drops to 0.9 at time scale of five years, which could relate to vegetation metabolism (see Figure 1b and the Discussion section). It is noted that care should be made when extrapolating the linear scaling since it can be meaningless at small or large timescales. In other words, the scaling obtained here is approximately valid in the range 1–6 years and should not to be extrapolated to less than 1 year and more than a decade. The use of a univariate linear regression to detect the scaling is parsimonious since the elasticity tendency is quantified by one parameter. Of course, the tendency could be estimated by more complex models.

For the attribution of the scaling to potential causes, in a first step we conducted a univariate attribution analysis, where we plotted the correlations between the scaling magnitude and catchment attributes. These can be used to detect the direct relationship between the two. In addition, we analyzed the cumulative distribution function (cdf) of the scaling in terms of the catchment attributes, which is used to detect whether there exists a noticeable scaling difference between different bins of samples classified using the various catchment attributes.

In a second step, we used a machine learning approach, the Regression Tree Ensemble (RTE; M. Li et al., 2020; Zhang et al., 2018) to predict the scaling magnitude and signs of scaling. This approach allows evaluating the relative importance of prediction factors. We used ten-fold spatial validations to test its predictability. Two steps are included: (a) all data were randomly divided into 10 groups; (b) one group was selected as the validation sample and the rest was used for building the RTE model, which was looped 10 times until all data were evaluated for validation. Based on the RTE model so estimated we conducted an importance analysis for each of the 18 predictive variables (i.e., catchment attributes; Zhang et al., 2018).

We used two metrics to evaluate model calibration and cross-validation performances: R^2 and hit rate. They are defined as follows:

$$R^2 = \left(\frac{\sum_{j=1}^{N} (S_j - \overline{S})(O_j - \overline{O})}{\sqrt{\sum_{j=1}^{N} (S_j - \overline{S})^2 \sum_{j=1}^{N} (O_j - \overline{O})^2}} \right)^2 \tag{3}$$

where R^2 is the coefficient of determination between the simulated streamflow elasticity (or, alternatively, the scaling of ε_{Pi}) from the RTE model (S) and that obtained from observed data (O), j is the catchment index, and N is the total number of catchments ($N = 5{,}327$). R^2 is also used as the metric of the importance analysis.

For analyzing the signs of the scaling of ε_{Pi}, we grouped the catchments into three categories: significantly positive ($p \leq 0.05$), significantly negative ($p \leq 0.05$), and non-significant ($p > 0.05$), based on the Student's t test on the regression slope. We evaluated the RTE hit rate using the following equation:

$$\mathrm{Acc}_k = \frac{C_{\mathrm{RTE},k}}{C_{O,k}} \times 100\% \tag{4}$$

where Acc_k is the hit rate of the RTE approach for the category k (e.g., "positive" scaling), $C_{O,k}$ is the total count of observed scaling of ε_{Pi} falling into the category k, $C_{\mathrm{RTE},k}$ is the count of RTE estimated scaling values which fall into the correct category k (i.e., number of the correctly classified sites).

It is noted that at dry catchments, monthly or subannual data can be skewed toward zero since sub-annual streamflows can remain close to zero, which can influence the elasticity estimates. However, there is no zero precipitation or streamflow issue at long timescales (annual or more) for the 5,327 selected catchments. This paper is interested in timescales from annual to decadal, and the sub-annual elasticities given in Figures 2 and 3a are there for completeness.

3. Results

3.1. Detection of Scaling

Figure 3 shows the estimated elasticities of streamflow to precipitation and its scaling for the 5,327 catchments included in the global analysis. Figure 3a shows how the elasticity varies with aggregation time in terms of its

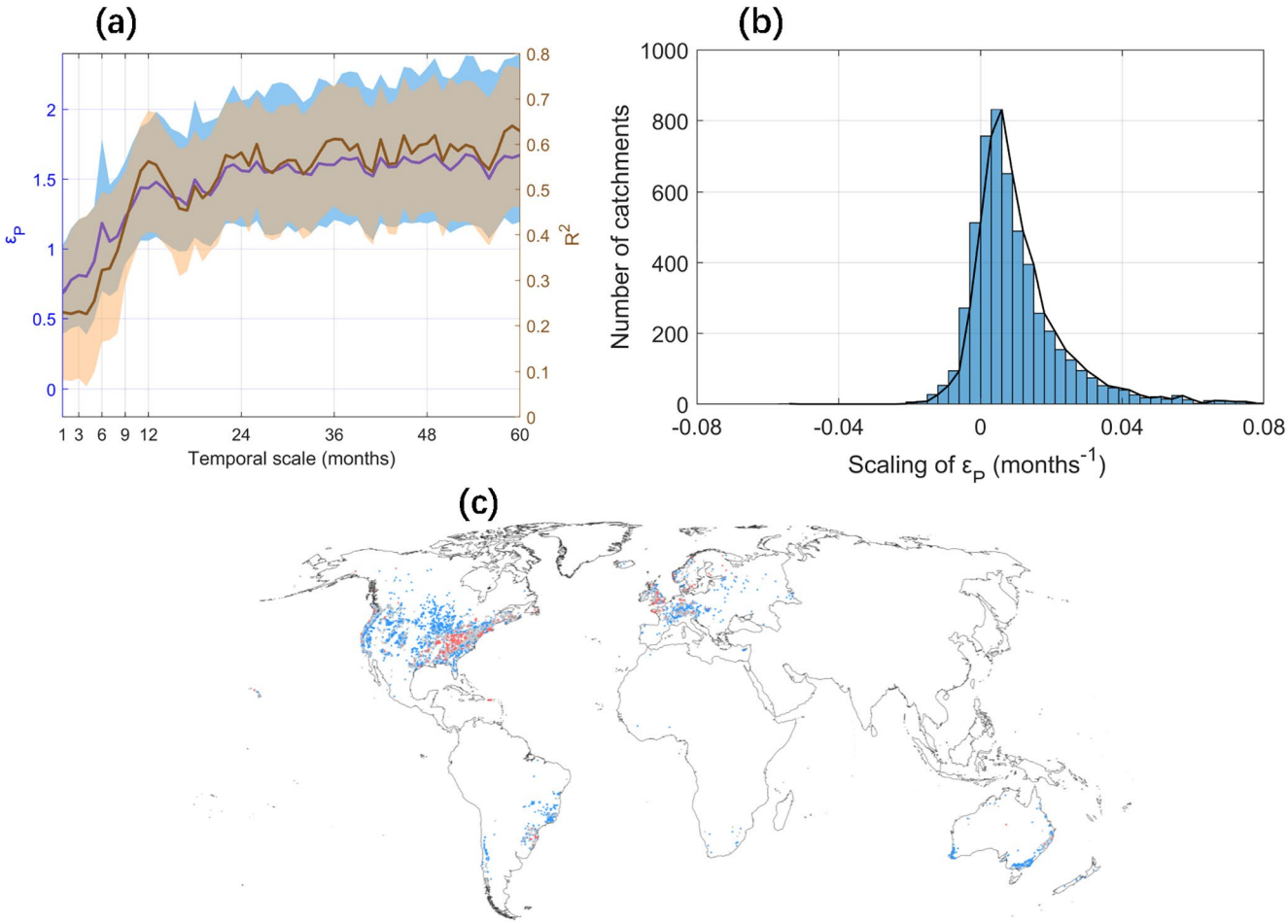

Figure 3. Scaling of elasticity. (a) Elasticity of streamflow to precipitation, as a function of aggregation time scale with the blue line indicating mean and the blue area ±1 s. dev. Of the spatial variability; Correlation R^2 between precipitation and streamflow as a function of aggregation time with the brown line indicating mean and the brown area ±1 s. dev. Of the spatial variability. (b) Histogram of the scaling of elasticity values; (c) global map of the scaling (blue: positive, red: negative, gray: non-significant).

average (thick blue line) and its spatial spread (light blue area). As expected, the streamflow elasticity to precipitation is lower at the seasonal timescale (for aggregation times of 1–12 months), which may be explained by catchment storage of water in soils, aquifers, snowpack and the landscape. This is because ε_{Pi} compares rainfall and streamflow of the same time step. For example, if a large portion of rain in a given month is stored in the catchment, only a small fraction of its effect on streamflow will appear in the same month and hence ε_{Pi} is small, while the remainder of the rainfall not evaporated will affect a later month not counted in the evaluation of ε_{Pi}. At the annual and multiannual timescales (for aggregation times of 12–60 months) the elasticity is larger and varies less, with average values approaching 1.5, even though a slight increase with aggregation time can be observed, on average, considering all catchments. The brown line and shaded area in Figure 3a show the mean and spatial spread of the coefficient of determination R^2 between precipitation and streamflow as a function of aggregation time. The shape of the functional dependence of R^2 on aggregation time is similar to that of the elasticity which would be expected as both are measures of the dependence of the two variables. The average value of R^2 is around 0.6 for annual and multiannual timescale, when the R^2 mainly varies between 0.4 and 0.7 across the 5,327 selected catchments. This indicates that about 60% of the temporal variance of streamflow can be explained by the temporal variability of precipitation.

Figures 3b and 3c show the scaling of the streamflow elasticity with timescale, that is, the tendency for the estimated elasticity to change with aggregation times from 13 to 60 months for the 5,327 catchments considered in the analysis. Figure 3b is the histogram of the scaling values, which suggests that, even though in most catchments

the scaling is close to 0, there are more catchments with a positive scaling than with a negative one. A positive scaling means that the sensitivity of streamflow to precipitation increases with the aggregation time interval (within the range 13–60 months), while a negative scaling means that it decreases. As shown in Figure 3b, the scaling of elasticity is basically distributed between −0.08 and 0.08 months^{-1}. If the scaling is out of this range, it is probably unrealistic and could lead to mass balance problems. The location of the catchments with significant positive (blue), significant negative (red), and non-significant (gray) scaling is shown in Figure 3c. Notwithstanding the considerable amount of scatter, some patterns can be observed in Figure 3c, such as the positive scaling in the Midwest of the United States, in Eastern Europe and in Southern Australia, and the negative scaling in the Eastern United States, and in Nord and Nord-Western Europe.

Overall, out of the 5,327 catchments considered, 3,182 (60%) have a significant positive scaling, 323 (6%) have a significant negative scaling, and 1,822 (34%) have non-significant scaling at a 5% significance level. The number of catchments showing a significant scaling of streamflow elasticity to precipitation with aggregation time is therefore much larger than expected by chance alone (i.e., 66% in total as opposed to 10% by change comprising 5% positive and 5 negative). This result, and the spatial patterns shown in Figure 3c, seem to suggest that a scaling of elasticity is not just an artifact of the limited record lengths, and it is therefore of interest to understand why these patterns emerge. In the following sections we perform a data analysis in the attempt to attribute the sign and magnitude of the scaling of streamflow elasticity to the driving causes.

3.2. Univariate Attribution of Scaling

For each catchment, a number of climatic, hydrologic and physiographic characteristics are available (see Table 1). Figure 4 shows, as scatterplots, the relationship between these catchment attributes and the scaling of streamflow elasticity to precipitation. The Pearson correlation coefficients are also indicated. For comparison, the bottom-right panel shows the correlation between the scaling and the mean elasticity (averaged over all aggregation times from 13 to 60 months). There is a clear dependence of the scaling on the magnitude of the elasticity itself, that is, larger elasticities correspond to larger scaling values, with a correlation coefficient larger than 60%. On the other hand, the dependence of the scaling on the individual catchment attributes is rather weak. Only precipitation, forest ratio and leaf area index exhibit correlation coefficients larger than 20% (in absolute value). All correlations are negative, suggesting that drier catchments located in the south with smaller areas of vegetation are characterized by a larger (more positive) scaling of streamflow elasticity to precipitation with aggregation time. It is noted that some attributes, such as precipitation, forest ratio and leaf area index can be highly correlated and their relative contributions to the elasticity value and its scaling are further analyzed in Section 3.3.

Even though the correlation between the magnitude of the scaling and the catchment attributes is rather low, some interesting relationships can be observed by comparing the distributions of these attributes for the ensembles of catchments with significant positive, significant negative and non-significant scaling values (i.e., signs indicated in Figure 3c for each catchment). Figure 5 shows the four attributes where these distributions differ the most: mean annual precipitation, aridity index, forest ratio, and mean slope. The difference test with Two-sample Kolmogorov-Smirnov method indicates the distributions of the four attributes are significantly ($p < 0.01$) different between significant positive scaling and significant negative scaling (or non-significant scaling). Significant negative scaling and non-significant scaling do have significant difference for the distributions of mean annual precipitation, aridity index, mean slope, but not for the distribution of forest ratio. The distribution of mean annual precipitation is shifted toward lower values for catchments characterized by a positive scaling, compared to all other catchments and, consistently, the distribution of the aridity index is shifted toward higher values for the same catchments. This means that more arid/less rainy catchments are more frequently characterized by a positive scaling of the streamflow elasticity to precipitation with aggregation time. Similarly, vegetation seems to have some explanatory power in determining the sign of the scaling. The distribution of the forest ratio is shifted toward lower values for catchments characterized by a positive scaling. The distributions differ the most for catchments with small forest ratios. The less forested catchments are more frequently characterized by a positive scaling. In the more forested catchments, the difference in frequency between positive and negative scaling is small. In terms of mean slope, the catchments with lower slope or more gentle terrain are more frequently characterized by a positive scaling.

Through this univariate analysis, some catchment attributes seem related to the sign and (less so) to the magnitude of the scaling of the streamflow elasticity to precipitation with aggregation time. However, it is difficult to

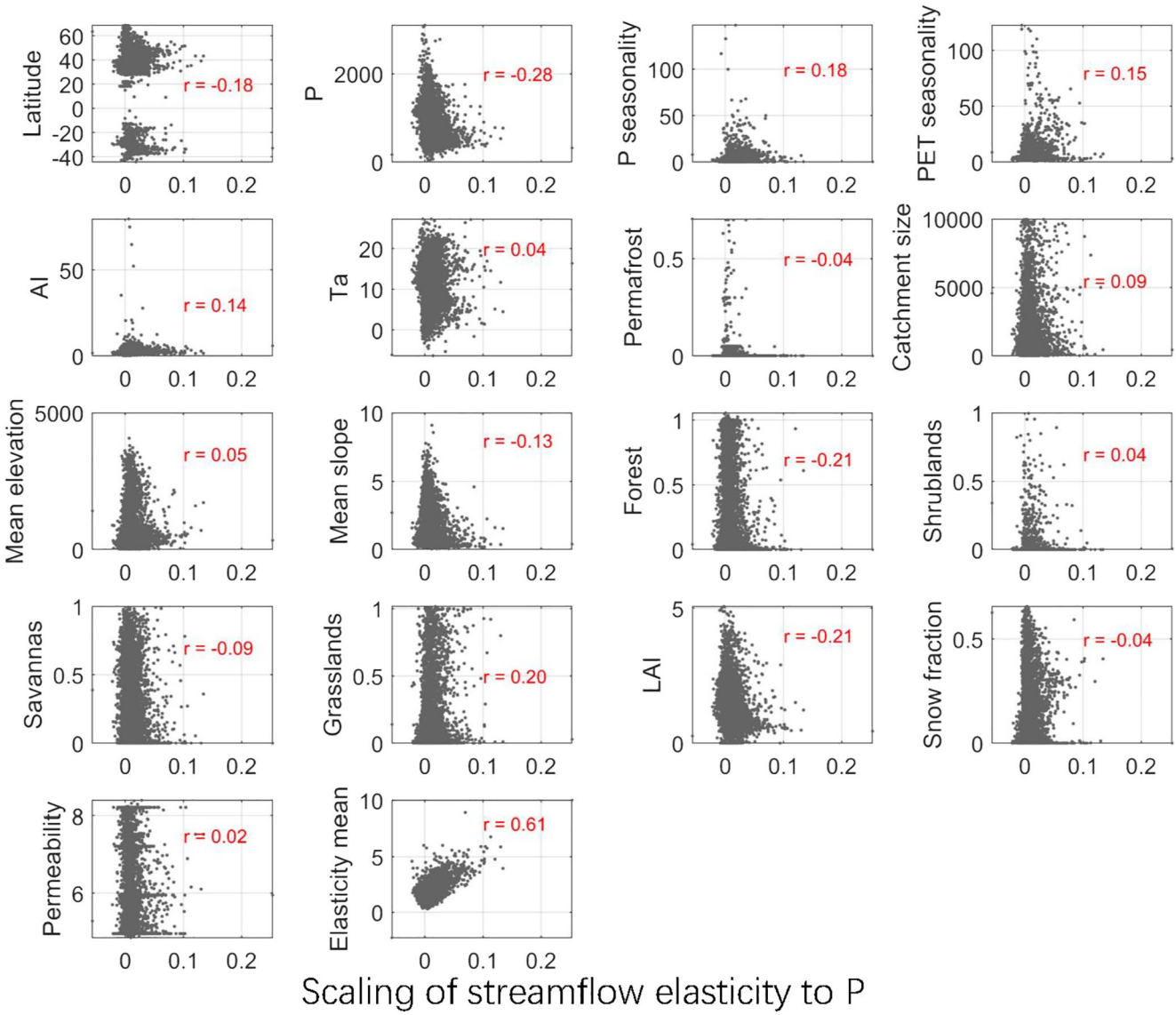

Figure 4. Correlation scatterplot between scaling of streamflow elasticity to precipitation (horizontal axes) and catchment attributes (vertical axes). Each point represents one catchment. Bottom right panel shows the mean elasticity versus its scaling. For definition and units of catchment attributes see Table 1. Numbers in red are the Pearson correlation coefficients.

identify which attributes are jointly influencing the scaling because they may be correlated among themselves. For example, forest ratio is correlated with precipitation, and precipitation with aridity, which may partly explain the finding that less forested catchments more frequently exhibit positive scaling. To evaluate the joint relation between more catchment attributes and the scaling of streamflow elasticity to precipitation, in the next section we perform a multivariate correlation analysis.

3.3. Multivariate Attribution of Scaling

Figure 6 shows the outcomes of the importance analysis described in Section 2.2. Figure 6a reports, as a reference, the amount of variance of the mean streamflow elasticity (averaged over all aggregation times from 13 to 60 months) that can be explained by random-forest regression models with one to 18 explanatory variables (i.e., catchment attributes). The red line shows the explanatory power of the models in calibration mode, while the blue line refers to the cross-validation mode, which is a measure of the prediction power of the model when used for "ungauged" catchments. While the best univariate model, with mean annual precipitation as the explanatory

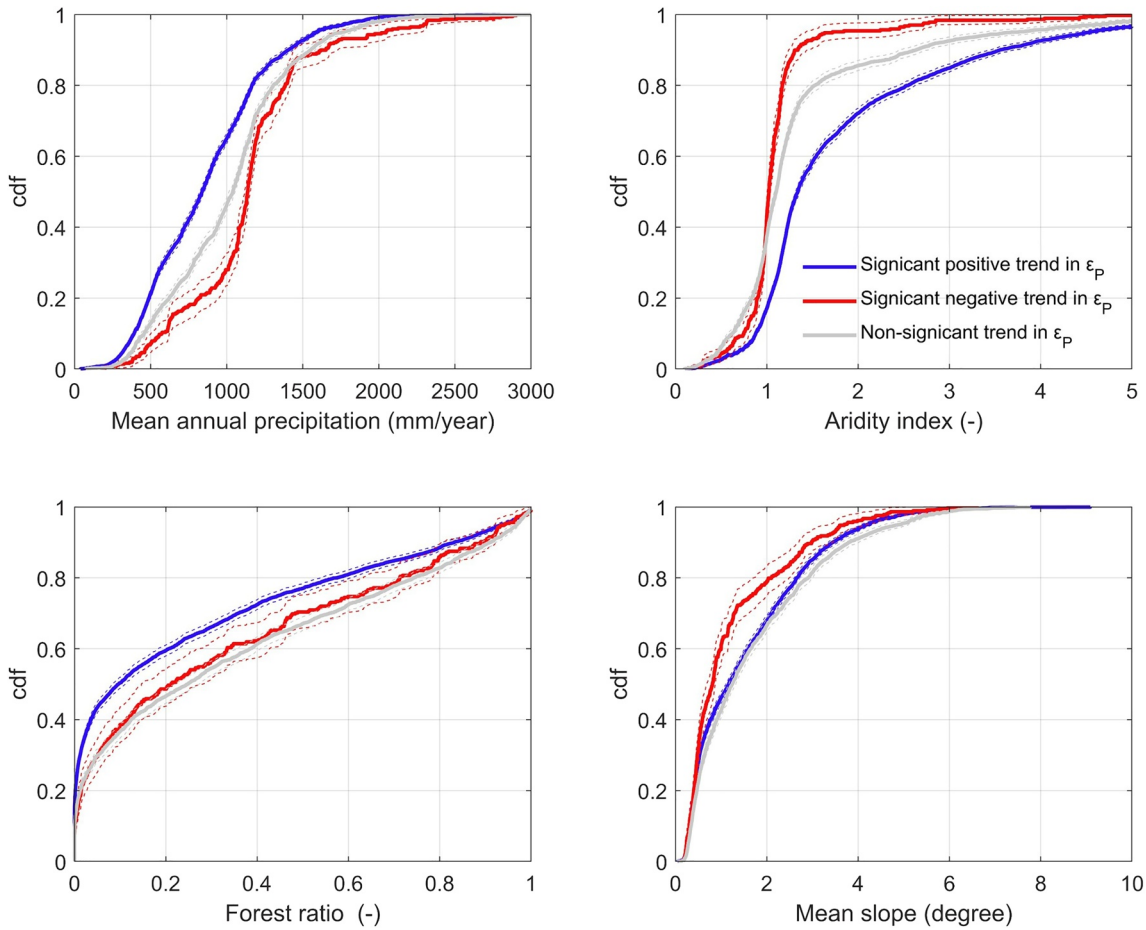

Figure 5. Cumulative distribution function (cdf) of catchment attributes stratified by the sign of the scaling of streamflow elasticity to precipitation. Dash lines are the 90% confidence intervals obtained using Greenwood's formula, which is an approximation for the variance of the Kaplan-Meier estimator.

variable, explains only about 20% of the spatial variance of elasticity, the model with three explanatory variables (i.e., mean annual precipitation, latitude and aridity index) explains more than 80% of it in calibration mode and almost 60% in validation mode. More complex models also including the seasonality of precipitation, catchment mean slope and mean elevation explain 90% of the spatial variance of elasticity in calibration mode and 70% in validation mode. The spatial variation of streamflow elasticity to precipitation at the global scale is thus mainly explained by climate but also catchment attributes play some role.

The importance analysis for the scaling of streamflow elasticity to precipitation with aggregation time is shown in Figure 6b. Even though the model with three explanatory variables explains about 70% of its variance in calibration, the cross-validation performance indicates that the prediction power of such a model is low, reaching an R^2 of about 40% which does not improve significantly with more explanatory variables. This suggests that the attribution of the magnitude of the scaling is not robust. As for the univariate analysis in Section 3.2, the magnitude of the scaling is not predicted well by the catchment attributes available in the database. However, its sign may be. Therefore, we also perform an importance analysis to identify whether a model can be found that explains the sign of the scaling of streamflow elasticity to precipitation with aggregation time.

Figure 6c presents the accuracy of random-forest classification models to identify the observed sign of the scaling. Dashed lines indicate the accuracy (i.e., percentage of catchments assigned to the right class) in calibration mode. With a univariate model having aridity index as explanatory variable, about 80% of the catchments with positive scaling and more than 35% of the catchments with non-significant scaling are classified as such. However almost no catchments with negative scaling are correctly classified by the model using aridity index alone. Multivariate models have a much higher accuracy, such as the five-variable model (i.e., aridity index, latitude, seasonality of

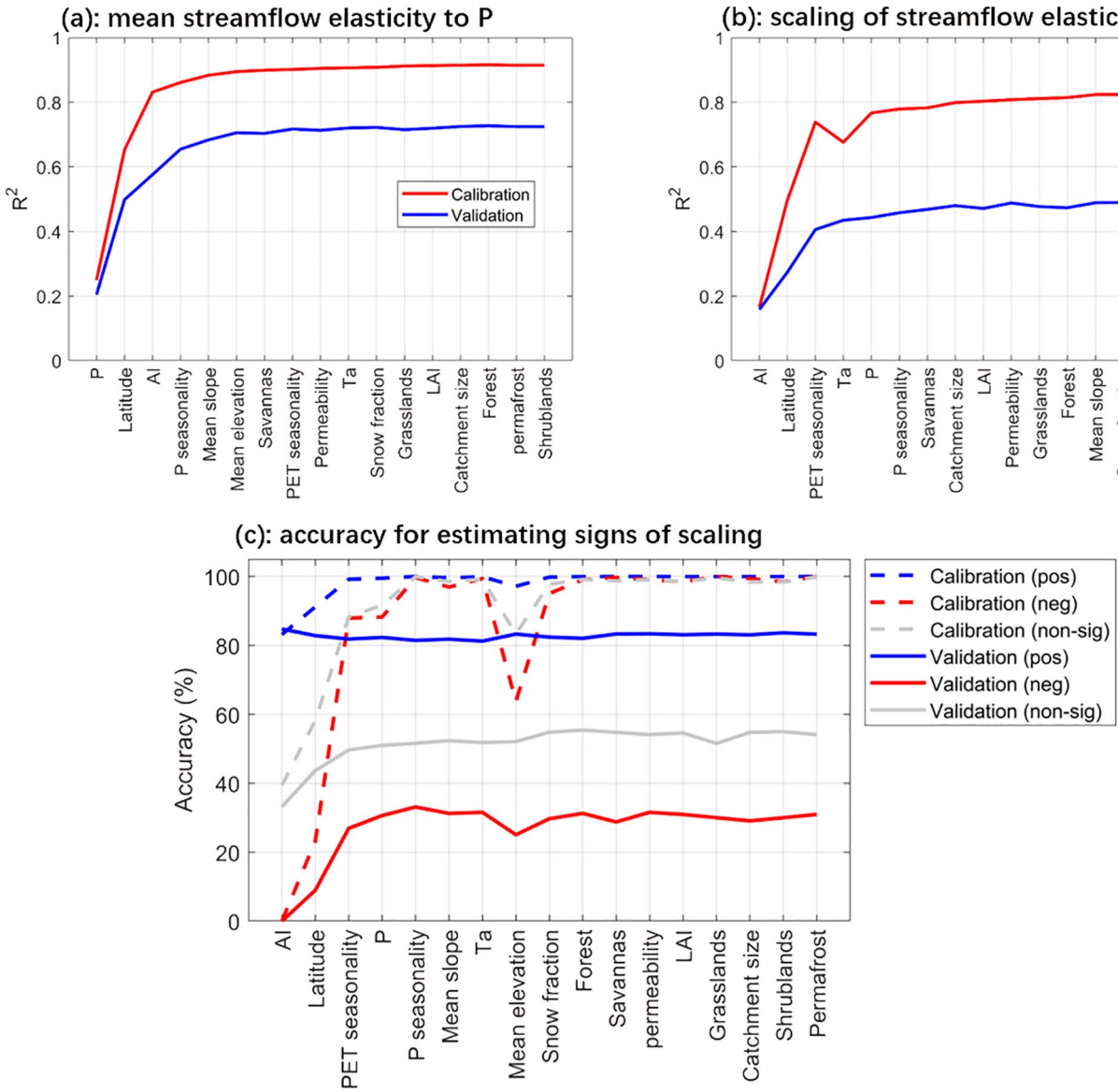

Figure 6. (a). Importance analysis (including cross-validation) for estimating the value of the mean elasticity of streamflow to precipitation. Attributes are sorted according to relative importance where the first attribute refers to a univariate model and the following attributes to multivariate models with increasing number of explanatory variables; (b). Importance analysis for estimating the value of the scaling of the elasticity; (c) Importance analysis for estimating the sign of the scaling of the elasticity. R^2 represents the coefficient of determination between the simulated streamflow elasticity of streamflow (or, alternatively, scaling of) from the RTE model and that obtained from observed data (Equation 3), and the accuracy represents the percentage of catchments assigned to the correct class (Equation 4).

the potential evapotranspiration, annual precipitation and seasonality of precipitation) that, in calibration mode, assigns to almost all of the catchments the right sign of the scaling. However, this accuracy decreases in cross-validation mode. While 80% of the catchments with positive scaling and 52% of the catchments with non-significant scaling are classified as such, less than 38% of the catchments with negative scaling are correctly classified by the model. The positive and non-significant scaling catchments can be predicted reasonably well, but not so the catchments with negative scaling. The analysis therefore suggests confidence in the data-based attribution of the non-negative scaling. As for the sign of elasticity, climate is the primary attribute responsible of its spatial variability at the global scale.

Given that no model could reasonably explain the spatial variability of the scaling magnitudes but some skill exists for models explaining their sign, it is of interest to investigate whether it is possible to attribute the causes for the spatial variability of the scaling when stratifying the catchments by its sign. This is especially interesting

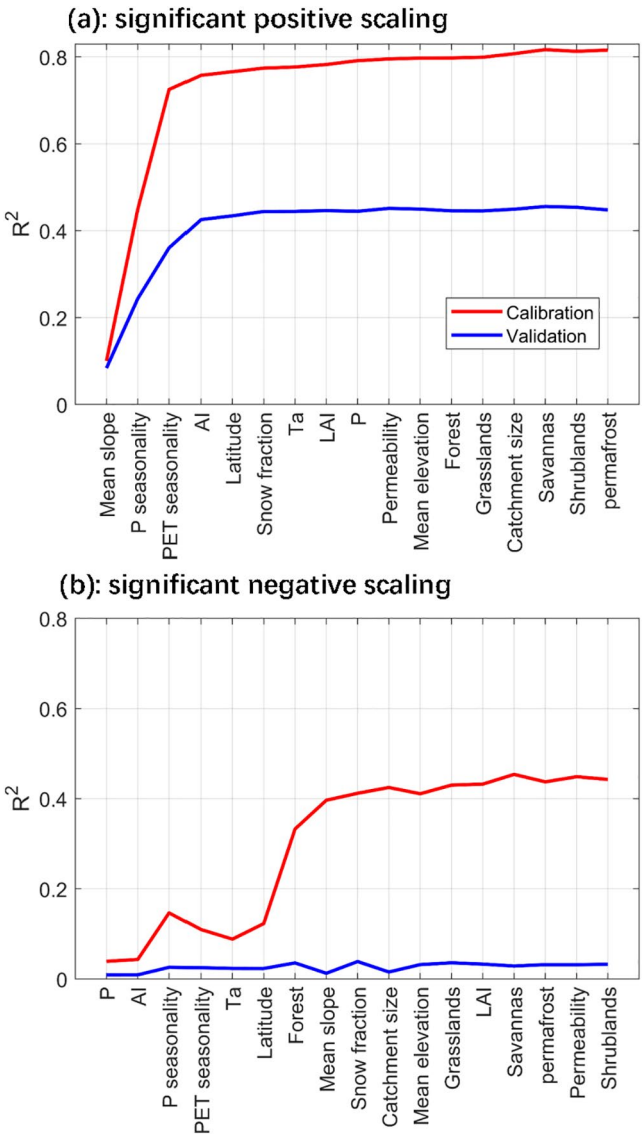

Figure 7. Similar to Figure 6b but separately for catchments with positive (a) and negative (b) scaling values.

for the catchments with positive scaling, which can be classified well by the random-forest classification model based mainly on climate variables. The results of this additional analysis are presented in Figure 7a which shows the importance analysis for the prediction of the value of the scaling for those catchments where the elasticity is significantly positive. The random-forest regression model with four explanatory variables (i.e., mean catchment slope, seasonality of precipitation, seasonality of potential evapotranspiration, and aridity index) explains more than 70% of the scaling variability in calibration mode and almost 40% of it in cross-validation mode. Even if this is not a very robust model, its performance is better than the performance of models explaining the full variability of the scaling (i.e., independently of its sign, in Figure 6b. On top of climatic variables, also a physiographic variable (mean catchment slope) appears in the best model. As expected, the performance is very low for catchments with significant negative scaling meaning that, on top of non being able to predict whether a catchment has a negative scaling, we are even less able to predict how negative it is, which is consistent with the previous analyses.

4. Discussion

In this paper, we use a data-based approach to investigate whether a scaling of streamflow elasticity to precipitation with aggregation time exists and, if so, to attribute the causes. We use precipitation only to evaluate the elasticity of runoff to precipitation with aggregation time from one year to multiple years (or a decade). It has been demonstrated in Figure 3a that, using precipitation only can explain 40%–70% variability of streamflow across the 5,327 catchments once the temporal scale reaches one year or more. This indicates that overall the 0.25°resolution of PGF data precipitation data is sufficient for the modeling and data analysis. Adding other contributors such as potential evapotranspiration and groundwater storage can have a secondary contribution to the streamflow variability (de Lavenne et al., 2021; Fu et al., 2007; Konapala & Mishra, 2016; Tang et al., 2020).

Based on statistical tests, we detect the presence of the scaling of streamflow elasticity to precipitation in a significant number of catchments around the world. Overall, out of the 5,327 considered catchments, 3,182 (60%) have a significant positive scaling and 323 (6%) have a significant negative scaling at a 5% significance level. The number of catchments showing a significant positive scaling of streamflow elasticity to precipitation with aggregation time is therefore much larger than expected by chance alone (i.e., 10% or 533 catchments). Even though the assumption of independence of the samples is not met at all sites, since some of them have serially correlated time series, the much large number of catchments with significant scaling than chance suggests that the scaling is real rather than an estimation artifact. Similarly, the larger number of catchments with positive scaling than those with negative scaling seems to be real. The implicit assumption usually made in climate impact analyses that elasticity does not depend on time scale may thus not be valid. In other words, streamflow response to, say, decadal climate fluctuations may be different from streamflow response to annual climate fluctuations. An anomalously wet decadal period may transform in a larger (or in some cases smaller) streamflow increase than an anomalously wet year. This finding should be taken into account when using elasticity in climate impact research (Fu et al., 2007; Yang & Yang, 2011).

Having detected the existence of both positive and negative scaling of streamflow elasticity to precipitation with aggregation time, we examine whether it can be attributed to physical causes using a comparative hydrology approach (Bloschl et al., 2013; Falkenmark & Chapman, 1989). We search for climate and catchment attributes that can explain the differences in scaling of streamflow elasticity to precipitation observed in the 5,327 catchments by correlation and importance analyses. No single characteristic is correlated well to the scaling values of

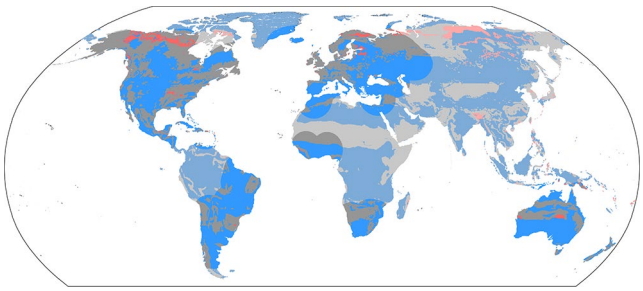

Figure 8. Global map of the predicted sign of the scaling of elasticity with aggregation time with the random forest model with 4 climate variables (AI, lat, PET seasonality and P). Blue denotes significant positive scaling; red denotes significant negative scaling; gray denotes insignificant scaling at the 5% level. Lighter colors for the same sign of scaling mean that the prediction points are more than 1000 km from any stream gauge (Figure 3c).

individual catchments, which are only positively correlated with the (mean) elasticity itself. However, if one considers an ensemble of catchments, that is, stratifying the catchments by the sign of the scaling, four attributes show interesting differences in their distributions. More arid/less rainy catchments are more frequently characterized by a positive scaling of the streamflow elasticity to precipitation with aggregation time. This may be due to the fact that arid catchments are characterized by larger elasticity (Sankarasubramanian et al., 2001) that, as mentioned above, is correlated to its scaling with aggregation time. Also, the less forested catchments are more frequently characterized by a positive scaling, which may be correlated with lower precipitation and larger aridity. The finding that the more forested catchments tend to be associated with negative scaling could be related to the way forest vegetation manages soil structure and its water holding capacity as well as transpiration (Bouaziz et al., 2020; Runyan et al., 2012; Troch et al., 2015). It is possible that the negative scaling reflects the effect of a type of metabolism, that is, the regulation capacity of the vegetation to transpire more water if the past years have been wet. However, more research is needed to test this hypothesis at the catchment scale. Finally, the catchments with higher contributions of baseflow to streamflow are more frequently characterized by a positive scaling. This can be related to the effect of catchment storage acting also at the multiannual timescale and determining the increase of elasticity, in a similar way as it does more visibly at the sub-annual timescale. This interpretation is consistent with multiscale analyses of long streamflow records which usually consider catchment storage as one of the reasons for the presence of long-range dependence (Montanari, 2003; Szolgayova et al., 2014).

Multivariate non-linear models are used to identify which attributes are jointly influencing the scaling. We find that some models seem to identify quite well the sign of the scaling, in particular whether a catchment has a non-negative scaling (positive or no-scaling). The best multivariate random forest classification model includes, as explanatory variables, aridity index, latitude, the potential evapotranspiration seasonality, air temperature, mean annual precipitation, and the precipitation seasonality. The model is mainly based on climate related attributes. This is consistent with the observation of the scaling being correlated with elasticity itself, whose global variability is mainly explained by climate (Chiew, 2006). However, the multivariate non-linear models based on machine learning used in this study do not allow distinguishing the individual contributions of the variables. To assist in the interpretation, Figure 8 shows how the model based on aridity index, latitude, seasonality of the potential evapotranspiration and mean annual precipitation, whose performance in validation is close to the best model, predicts the sign of the scaling globally. The figure should not be used for predictive purposes but merely as a means for exploring the characteristics of a model that captures quite well whether a catchment has a positive scaling or no-scaling (blue and gray regions in the figure).

Figure 8 indicates that drier and warmer regions tend to exhibit more positive scaling (e.g., the Mediterranean area, Australia, the Mid West of the United States). Australia is not only dry, but also characterized by large intra-annual variability due to climate modes. Therefore, it is expected that the long-term water balance and very slow runoff (i.e., base flow contributed by groundwater storage) are more affected by climatic change than faster runoff processes in the regions with positive scaling.

It is possible that the prevailing positive scaling is related to the role of climate modes, in particular if the runoff response to climate is non-linear with disproportionate or threshold effects as suggested by data analyses in Australia (Peterson et al., 2009, 2012). While Australia is also an area where the elasticity of streamflow to precipitation is itself high (see Figure 3 in (Chiew, 2006)), this is less so the case in the Mediterranean area and Mid West of the US pointing to the role of climate modes in Australia. High latitudes in the North, that is, dry and cold regions, more likely have non-positive or negative scaling. For instance, the non-positive scaling observed in Canada or Northern Europe may be related to snow processes and the decadal periodicity of energy availability. At the scale of decades, it may no longer be the storage of water that is relevant to scaling in these catchments but negative correlations between precipitation and air temperature, that is, the tendency for periods of higher precipitation to be associated with periods of lower temperature and thus less snow melt. The presence of such negative correlations between precipitation and temperature depends on the region and the season and may be

caused by the fact that a large frequency of cyclones implies more precipitation, more cloud cover and less solar radiation and thus lower temperatures (Blöschl et al., 2020; Gagen et al., 2016). Note that the model is not very accurate in predicting negative scaling (Figure 7c), indicating that complex physical processes may control it and more in-depth research is required. Interestingly, one can also notice that the equatorial zone characterized by forests, warm climate, and high and strongly seasonal precipitation exhibits, in general, less positive scaling. The role of forests is not completely clear and more researches on this should be carried out in the future. In fact, a potential metabolism effect of vegetation, which individually would cause negative scaling, may contribute to the less positive scaling in these regions.

While the sign of the scaling of streamflow elasticity to precipitation with aggregation time is mainly controlled by climate, the spatial variability of the scaling magnitudes when the scaling is positive is also related to a physiographic variable, that is, mean catchment slope, which appears as first controlling variable in the multivariate random forest regression model. It is possible that catchment slope is a proxy of other processes or characteristics such as the subsurface storage capacity or topographic effects on climate.

The scaling concept developed here is perhaps too simple for being used in practice as predictive model to support water management policies. This paper simply analyzes how the observed elasticity of streamflow to precipitation may depend on the timescale and what could be the causes of this dependency. However, the usefulness of this analysis can be manyfold. We give several examples. First, it can be used to detect catchment evolution with climate variability and climate change across the regional and global scales, as shown in Figure 8. Second, it is useful for investigating effects of changing sign of the scaling of elasticity under the anthropogenic impacts. Third, it can also be used to check and improve global coupled climate-hydrologic models in the case that they are far from reproducing this scaling of the elasticity. Also, increasing elasticity with timescale may indicate hydrologic memory which can exacerbate the effects of climate change in certain parts of the world.

5. Conclusions

Based on the analyses of streamflow records in 5,327 selected catchments around the world over the period 1950–2016 we draw the following conclusions.

1. A significant scaling of streamflow elasticity to precipitation with aggregation time (from 13 to 60 months) is detected in 66% of the catchments (5% significance level) which is much larger than expected by chance (10%)
2. The catchments with significant positive scaling of elasticity (59%) are more frequent than those with significant negative scaling of elasticity (6%)
3. For individual catchments, catchment attributes do not show significant univariate correlations with the scaling of elasticity, but for an ensemble of catchments, that is, when stratifying the catchments by the sign of the scaling, more arid/less rainy catchments, less forested catchments and catchments with a large baseflow contribution to streamflow are more frequently characterized by a positive scaling
4. A multivariate analysis, using a random forest classification model, identifies aridity index, latitude, the potential evapotranspiration seasonality, air temperature, mean annual precipitation, and the precipitation seasonality as relevant explanatory variables of the scaling of elasticity
5. A global mapping of the scaling of elasticity allows interpreting the sign of the scaling by non-linear runoff generation in arid regions, by the effect of climate modes and snow processes, and by the regulation capacity of vegetation to transpire more water if the past years were wet
6. It is suggested that the scaling of streamflow elasticity to precipitation with aggregation time should be considered when using elasticity in climate impact analyses, that is, instead of annual elasticities, decadal elasticities should be used

Data Availability Statement

Streamflow data used for this study were obtained from various agencies and their relative links have been provided in method section. Precipitation data were obtained from Princeton Global Forcing data set that is publicly available at https://hydrology.princeton.edu/data.pgf.php. We thank anonymous reviewers and editors for their critical and constructive comments on this paper.

Conflict of Interest

The authors declare no conflicts of interest relevant to this study.

Acknowledgments
This study was supported by the CAS Talents Program, the National Natural Science Foundation of China (Grant No. 41971032), the Second Tibetan Plateau Scientific Expedition and Research Program (2019QZKK0208), and the Austrian Science Funds (project No. I 3174 and I 4776). We thank Hylke Beck, Hongxing Zheng, Yuhan Guo and Xuanze Zhang for collating datasets used for our global analysis.

References

Andermann, C., Longuevergne, L., Bonnet, S., Crave, A., Davy, P., & Gloaguen, R. (2012). Impact of transient groundwater storage on the discharge of Himalayan Rivers. *Nature Geoscience*, *5*(2), 127–132. https://doi.org/10.1038/ngeo1356

Andreassian, V., Coron, L., Lerat, J., & Le Moine, N. (2016). Climate elasticity of streamflow revisited—An elasticity index based on long-term hydrometeorological records. *Hydrology and Earth System Sciences*, *20*(11), 4503–4524. https://doi.org/10.5194/hess-20-4503-2016

Apurv, T., Sivapalan, M., & Cai, X. M. (2017). Understanding the role of climate characteristics in drought propagation. *Water Resources Research*, *53*(11), 9304–9329. https://doi.org/10.1002/2017wr021445

Asbjornsen, H., Goldsmith, G. R., Alvarado-Barrientos, M. S., Rebel, K., Van Osch, F. P., Rietkerk, M., et al. (2011). Ecohydrological advances and applications in plant-water relations research: A review. *Journal of Plant Ecology*, *4*(3), 192. https://doi.org/10.1093/jpe/rtr005

Bao, Z., Zhang, J., Liu, J., Wang, G., Yan, X., Wang, X., & Zhang, L. (2012). Sensitivity of hydrological variables to climate change in the Haihe River basin, China. *Hydrological Processes*, *26*(15), 2294–2306. https://doi.org/10.1002/hyp.8348

Berghuijs, W. R., Hartmann, A., & Woods, R. A. (2016). Streamflow sensitivity to water storage changes across Europe. *Geophysical Research Letters*, *43*(5), 1980–1987. https://doi.org/10.1002/2016gl067927

Blöschl, G., Kiss, A., Viglione, A., Barriendos, M., Böhm, O., Brázdil, R., et al. (2020). Current European flood-rich period exceptional compared with past 500 years. *Nature*, *583*(7817), 560–566. https://doi.org/10.1038/s41586-020-2478-3

Bloschl, G., Sivapalan, M., Savenije, H., Wagener, T., & Viglione, A. (2013). *Runoff prediction in ungauged basins: Synthesis across processes, places and scales*. Cambridge University Press.

Bott, T. L., Newbold, J. D., & Arscott, D. B. (2006). Ecosystem metabolism in piedmont streams: Reach geomorphology modulates the influence of riparian vegetation. *Ecosystems*, *9*(3), 398–421. https://doi.org/10.1007/s10021-005-0086-6

Bouaziz, L. J. E., Steele-Dunne, S. C., Schellekens, J., Weerts, A. H., Stam, J., Sprokkereef, E., et al. (2020). Improved understanding of the link between catchment-scale vegetation accessible storage and satellite-derived soil water index. *Water Resources Research*, *56*(3), e2019WR026365. https://doi.org/10.1029/2019WR026365

Chiew, F. H. S. (2006). Estimation of rainfall elasticity of streamflow in Australia. *Hydrological Sciences Journal*, *51*(4), 613–625. https://doi.org/10.1623/hysj.51.4.613

Chiew, F. H. S., Peel, M. C., McMahon, T. A., & Siriwardena, L. W. (2006). Precipitation elasticity of streamflow in catchments across the world. In S. Demuth, A. Gustard, E. Planos, F. Scatena, & E. Servat (Eds.), *Climate variability and change—hydrological impacts* (pp. 256–262). IAHS.

Condon, L. E., & Maxwell, R. M. (2019). Simulating the sensitivity of evapotranspiration and streamflow to large-scale groundwater depletion. *Science Advances*, *5*(6), eaav4574. https://doi.org/10.1126/sciadv.aav4574

de Graaf, I. E. M., Gleeson, T., van Beek, L. P. H., Sutanudjaja, E. H., & Bierkens, M. F. P. (2019). Environmental flow limits to global groundwater pumping. *Nature*, *574*(7776), 90–94. https://doi.org/10.1038/s41586-019-1594-4

de Lavenne, A., Andréassian, V., Crochemore, L., Lindström, G., & Arheimer, B. (2021). Quantifying pluri annual hydrological memory with catchment forgetting curves. *Hydrology and Earth System Sciences Discussions*, 1–27. https://doi.org/10.5194/hess-2021-331

D'Odorico, P., Caylor, K., Okin, G. S., & Scanlon, T. M. (2007). On soil moisture-vegetation feedbacks and their possible effects on the dynamics of dryland ecosystems. *Journal of Geophysical Research*, *112*(G4). https://doi.org/10.1029/2006jg000379

Falkenmark, M., & Chapman, T. (1989). *Comparative hydrology: An ecological approach to land and water resources*.

Folland, C. K., Knight, J., Linderholm, H. W., Fereday, D., Ineson, S., & Hurrell, J. W. (2009). The summer North Atlantic oscillation: Past, present, and future. *Journal of Climate*, *22*(5), 1082–1103. https://doi.org/10.1175/2008jcli2459.1

Fu, G., Charles, S. P., & Chiew, F. H. S. (2007). A two-parameter climate elasticity of streamflow index to assess climate change effects on annual streamflow. *Water Resources Research*, *43*(11), W11419. https://doi.org/10.1029/2007wr00589010.1029/2007wr005890

Gagen, M. H., Zorita, E., McCarroll, D., Zahn, M., Young, G. H. F., & Robertson, I. (2016). North Atlantic summer storm tracks over Europe dominated by internal variability over the past millennium. *Nature Geoscience*, *9*(8), 630–635. https://doi.org/10.1038/ngeo2752

Gao, H., Hrachowitz, M., Schymanski, S. J., Fenicia, F., Sriwongsitanon, N., & Savenije, H. H. G. (2014). Climate controls how ecosystems size the root zone storage capacity at catchment scale. *Geophysical Research Letters*, *41*(22), 7916–7923. https://doi.org/10.1002/2014GL061668

Gleeson, T., Moosdorf, N., Hartmann, J., & Van Beek, L. (2014). A glimpse beneath earth's surface: GLobal HYdrogeology MaPS (GLHYMPS) of permeability and porosity. *Geophysical Research Letters*, *41*(11), 3891–3898. https://doi.org/10.1002/2014gl059856

Hofstatter, M., & Bloschl, G. (2019). Vb cyclones synchronized with the Arctic-/North Atlantic oscillation. *Journal of Geophysical Research: Atmospheres*, *124*(6), 3259–3278. https://doi.org/10.1029/2018jd029420

Huang, Z., Yang, H., & Yang, D. (2016). Dominant climatic factors driving annual runoff changes at the catchment scale across China. *Hydrology and Earth System Sciences*, *20*(7), 2573–2587. https://doi.org/10.5194/hess-20-2573-2016

IPCC. (2013). *Climate change 2013, the physical science basis*. Cambridge University Press.

Konapala, G., & Mishra, A. K. (2016). Three-parameter-based streamflow elasticity model: Application to MOPEX basins in the USA at annual and seasonal scales. *Hydrology and Earth System Sciences*, *20*(6), 2545–2556. https://doi.org/10.5194/hess-20-2545-2016

Li, M., Zhang, Y., Wallace, J., & Campbell, E. (2020). Estimating annual runoff in response to forest change: A statistical method based on random forest. *Journal of Hydrology*, *589*, 125168. https://doi.org/10.1016/j.jhydrol.2020.125168

Li, S. J., Wu, L. X., Yang, Y., Geng, T., Cai, W. J., Gan, B. L., et al. (2020). The Pacific Decadal Oscillation less predictable under greenhouse warming. *Nature Climate Change*, *10*(1), 30–34. https://doi.org/10.1038/s41558-019-0663-x

Li, Z., Chen, Y., Li, Y., & Wang, Y. (2020). Declining snowfall fraction in the alpine regions, Central Asia. *Scientific Reports*, *10*(1), 3476. https://doi.org/10.1038/s41598-020-60303-z

Liang, W., Bai, D., Wang, F., Fu, B., Yan, J., Wang, S., et al. (2015). Quantifying the impacts of climate change and ecological restoration on streamflow changes based on a Budyko hydrological model in China's Loess Plateau. *Water Resources Research*, *51*(8), 6500–6519. https://doi.org/10.1002/2014wr016589

Liu, J. Y., Zhang, Q., Zhang, Y. Q., Chen, X., Li, J. F., & Aryal, S. K. (2017). Deducing climatic elasticity to assess projected climate change impacts on streamflow change across China. *Journal of Geophysical Research: Atmospheres*, *122*(19), 10197–10214. https://doi.org/10.1002/2017jd026701

Lv, M., Ma, Z., & Lv, M. (2018). Effects of climate/land surface changes on streamflow with consideration of precipitation intensity and catchment characteristics in the yellow river basin. *Journal of Geophysical Research: Atmospheres*, *123*(4), 1942–1958. https://doi.org/10.1002/2017jd027625

Markonis, Y., Moustakis, Y., Nasika, C., Sychova, P., Dimitriadis, P., Hanel, M., et al. (2018). Global estimation of long-term persistence in annual river runoff. *Advances in Water Resources*, *113*, 1–12. https://doi.org/10.1016/j.advwatres.2018.01.003

Maxwell, R. M., & Condon, L. E. (2016). Connections between groundwater flow and transpiration partitioning. *Science*, *353*(6297), 377–380. https://doi.org/10.1126/science.aaf7891

Milly, P. C. D., Dunne, K. A., & Vecchia, A. V. (2005). Global pattern of trends in streamflow and water availability in a changing climate. *Nature*, *438*(7066), 347–350. https://doi.org/10.1038/nature04312

Montanari, A. (2003). Long–Range dependence in Hydrology. In P. Doukhan, G. Oppenheim, & M. S. Taqqu (Eds.), *Theory and applications of long–range dependence* (pp. 461–472). Birkhäuser.

NĚMec, J., & Schaake, J. (1982). Sensitivity of water resource systems to climate variation. *Hydrological Sciences Journal*, *27*(3), 327–343. https://doi.org/10.1080/02626668209491113

Peters-Lidard, C. D., Clark, M., Samaniego, L., Verhoest, N. E. C., van Emmerik, T., Uijlenhoet, R., et al. (2017). Scaling, similarity, and the fourth paradigm for hydrology. *Hydrology and Earth System Sciences*, *21*(7), 3701–3713. https://doi.org/10.5194/hess-21-3701-2017

Peterson, T. J., Argent, R. M., Western, A. W., & Chiew, F. H. S. (2009). Multiple stable states in hydrological models: An ecohydrological investigation. *Water Resources Research*, *45*(3). https://doi.org/10.1029/2008WR006886

Peterson, T. J., Western, A. W., & Argent, R. M. (2012). Analytical methods for ecosystem resilience: A hydrological investigation. *Water Resources Research*. (Vol. *48*). https://doi.org/10.1029/2012wr012150

Runyan, C. W., D'Odorico, P., & Lawrence, D. (2012). Physical and biological feedbacks of deforestation. *Reviews of Geophysics*, *50*(4). https://doi.org/10.1029/2012RG000394

Sankarasubramanian, A., Vogel, R. M., & Limbrunner, J. F. (2001). Climate elasticity of streamflow in the United States. *Water Resources Research*, *37*(6), 1771–1781. https://doi.org/10.1029/2000wr900330

Scanlon, B. R., Levitt, D. G., Reedy, R. C., Keese, K. E., & Sully, M. J. (2005). Ecological controls on water-cycle response to climate variability in deserts. *Proceedings of the National Academy of Sciences of the United States of America*, *102*(17), 6033–6038. https://doi.org/10.1073/pnas.0408571102

Scanlon, B. R., Zhang, Z., Save, H., Sun, A. Y., Müller Schmied, H., van Beek, L. P. H., et al. (2018). Global models underestimate large decadal declining and rising water storage trends relative to GRACE satellite data. *Proceedings of the National Academy of Sciences of the United States of America*, *115*(6), E1080–E1089. https://doi.org/10.1073/pnas.1704665115

Scheffer, M., Bascompte, J., Brock, W. A., Brovkin, V., Carpenter, S. R., Dakos, V., et al. (2009). Early-warning signals for critical transitions. *Nature*, *461*(7260), 53–59. https://doi.org/10.1038/nature08227

Sheffield, J., Goteti, G., & Wood, E. F. (2006). Development of a 50-year high-resolution global dataset of meteorological forcings for land surface modeling. *Journal of Climate*, *19*(13), 3088–3111. https://doi.org/10.1175/jcli3790.1

Sheffield, J., Wood, E. F., & Roderick, M. L. (2012). Little change in global drought over the past 60 years. *Nature*, *491*(7424), 435–438. https://doi.org/10.1038/nature11575

Sivapalan, M., & Bloschl, G. (2015). Time scale interactions and the coevolution of humans and water. *Water Resources Research*, *51*(9), 6988–7022. https://doi.org/10.1002/2015wr017896

Szolgayova, E., Laaha, G., Blöschl, G., & Bucher, C. (2014). Factors influencing long range dependence in streamflow of European rivers. *Hydrological Processes*, *28*(4), 1573–1586. https://doi.org/10.1002/hyp.9694

Takaku, J., Tadono, T., & Tsutsui, K. (2014). Generation of high resolution global DSM from ALOS PRISM. *ISPRS Annals of Photogrammetry, Remote Sensing Spatial Information Sciences*, *2*(4). https://doi.org/10.5194/isprsarchives-xl-4-243-2014

Tallaksen, L. M., Hisdal, H., & Van Lanen, H. A. J. (2009). Space-time modelling of catchment scale drought characteristics. *Journal of Hydrology*, *375*(3–4), 363–372. https://doi.org/10.1016/j.jhydrol.2009.06.032

Tang, Y., Tang, Q., & Zhang, L. (2020). Derivation of inter annual climate elasticity of streamflow. *Water Resources Research*, *56*(11), e2020WR027703. https://doi.org/10.1029/2020WR027703

Teutschbein, C., & Seibert, J. (2010). Regional climate models for hydrological impact studies at the catchment scale: A review of recent modeling strategies. *Geography Compass*, *4*(7), 834–860. https://doi.org/10.1111/j.1749-8198.2010.00357.x

Timmermann, A., An, S. I., Kug, J. S., Jin, F. F., Cai, W., Capotondi, A., et al. (2018). El Nino-southern oscillation complexity. *Nature*, *559*(7715), 535–545.

Troch, P. A., Lahmers, T., Meira, A., Mukherjee, R., Pedersen, J. W., Roy, T., & Valdés-Pineda, R. (2015). Catchment coevolution: A useful framework for improving predictions of hydrological change? *Water Resources Research*, *51*(7), 4903–4922. https://doi.org/10.1002/2015WR017032

Ukkola, A. M., Prentice, I. C., Keenan, T. F., van Dijk, A., Viney, N. R., Myneni, R. B., & Bi, J. (2016). Reduced streamflow in water-stressed climates consistent with CO_2 effects on vegetation. *Nature Climate Change*, *6*(1), 75–78. https://doi.org/10.1038/nclimate2831

Van Loon, A. F., & Laaha, G. (2015). Hydrological drought severity explained by climate and catchment characteristics. *Journal of Hydrology*, *526*, 3–14. https://doi.org/10.1016/j.jhydrol.2014.10.059

Yang, H., & Yang, D. (2011). Derivation of climate elasticity of runoff to assess the effects of climate change on annual runoff. *Water Resources Research*, *47*(7). https://doi.org/10.1029/2010WR009287

Zhang, Y., Chiew, F. H. S., Li, M., & Post, D. (2018). Predicting runoff signatures using regression and hydrological modeling approaches. *Water Resources Research*, *54*(10), 7859–7878, https://doi.org/10.1029/2018WR023325

Zheng, H., Zhang, L., Zhu, R., Liu, C., Sato, Y., & Fukushima, Y. (2009). Responses of streamflow to climate and land surface change in the headwaters of the Yellow River Basin. *Water Resources Research*, *45*(7), W00A19. https://doi.org/10.1029/2007WR00666510.1029/2007wr006665

Zhou, G. Y., Wei, X., Chen, X., Zhou, P., Liu, X., Xiao, Y., et al. (2015). Global pattern for the effect of climate and land cover on water yield. *Nature Communications*, *6*. https://doi.org/10.1038/ncomms691810.1038/ncomms6918

Zhou, X., Zhang, Y., Beck, H. E., & Yang, Y. (2021). Divergent negative spring vegetation and summer runoff patterns and their driving mechanisms in natural ecosystems of northern latitudes. *Journal of Hydrology*, *592*, 125848. https://doi.org/10.1016/j.jhydrol.2020.125848